

System Identification of Fused Filament Fabrication Additive Manufacturing Extrusion and Spreading Dynamics

Osama Habbal*, Ali Kassab**, Georges Ayoub**, Pravansu Mohanty*, Christopher Pannier*

*Department of Mechanical Engineering, University of Michigan-Dearborn, Dearborn, MI 48128

**Department of Industrial and Manufacturing Systems Engineering, University of Michigan-Dearborn, Dearborn, MI 48128

Abstract

In fused filament fabrication additive manufacturing, polymer extrusion and spreading dynamics affect build quality in both surface finish and mechanical properties. The state of the art in extrusion modeling and control is identification and compensation of a fixed first order pole with a linear model of the system. However, physical nonlinearities cause deviation of this pole in practice. To advance the aim of slicing using accurate nonlinear dynamic models, this work presents a system and procedure for automated measurement of dynamic bead extrusion. The system uses a belt printer, iFactory3D One Pro, with nozzle tilted 45 degrees from the build belt, and a snapshot 3D scanner. Single layer prints in polylactic acid (PLA) are scanned and then automatically ejected. The gcode for the single bead print holds the gantry speed fixed or extrusion speed constant while the extrusion flow rate or gantry speed is varied as a step input signal in space. The experiment design matrix varied two variables: gantry speed and extrusion flow rate. Time constants are fitted to bead area signals that are extracted from the scan data to obtain nonlinear models. Depending on the experiment condition, the percent difference between the highest time constant and the lowest time constant ranged from 279% to 61%, confirming the high nonlinearity of the extrusion system in FFF 3D printers. Additionally, measurements are performed on a cartesian 3D printer with a 2D scanner to test applicability of the methods to a general audience and verify observed trends. It was observed that larger steps in extrusion velocity for a constant X-Axis velocity, yielded smaller time constants, while the same steps in velocity using a constant extrusion velocity condition with variable X-Axis velocity, yielded the opposite trend. Moreover, the time constants for a step up in extrusion velocity yielded higher overall values in time constant when compared to step down conditions.

Introduction

Fused filament fabrication (FFF), a widely adopted 3D printing method, uses the controlled extrusion of thermoplastic materials in a layer-wise manner to construct objects from digital designs [1]. This technique offers versatility and scalability for a multitude of applications [2], [3]. In FFF printers, a motor feeds plastic filament from a spool into a heated liquefier where it undergoes melting. The resulting molten material extrudes through a nozzle. As the motorized stage moves the nozzle over the printing surface on a predetermined toolpath, a continuous thin strand or “bead” of extruded thermoplastic

polymer rapidly solidifies upon contact with the build plate or previously deposited layers. This layering process continues to form an object from perimeter beads and infill beads [4], [5].

Extrusion errors are a major cause of deviation between the printed part's geometry and the given 3D model. To understand extrusion behavior, the toolpath is divided into five phases: pre-movement, start-up, steady-state, slow-down, and exit-move. The initial phase, pre-movement, involves initiating a designated volumetric flow rate. In the start-up phase, polymer flow is accelerated inside the nozzle towards the steady state phase. The steady-state phase maintains a constant flow rate after the acceleration phase. During the slow-down phase, the flow rate goes to zero and even negative as a specified amount of material in the nozzle tip is reintroduced into the liquefier by reversing the motion of the rollers (see Figure 1) in a move called “retraction” of the filament. The final phase, exit-move, maintains zero flow rate and moves the nozzle to a predetermined distance from the last toolpath point to prevent interaction with the extruded material [4].

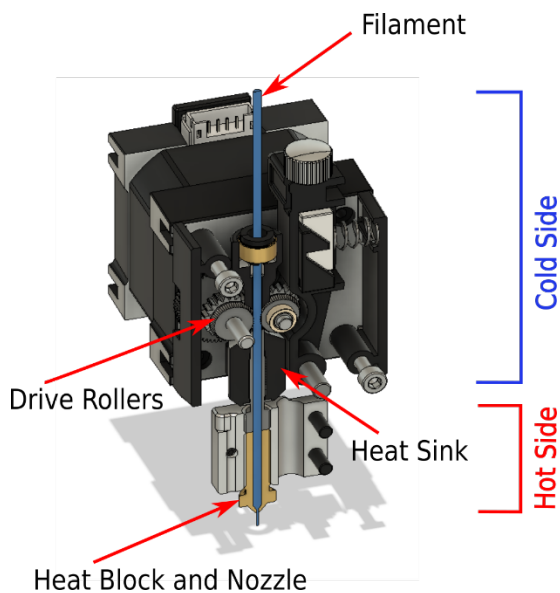


Figure 1. Extruder cross-sectional view of a E3D Hemera extruder with Volcano heat-block

Achieving precise and high-quality deposition relies on the crucial synchronization between the slow extrusion system and the fast motion system. Insufficient synchronization can lead to undesired effects such as over-extrusion, in which the flow rate exceeds the desired level, or under-extrusion, where the flow rate falls short of the desired level. These effects are particularly prominent during the acceleration and deceleration phases [6]. The dynamics of the fast motion system are reasonably linear, especially when conservatively low acceleration and feed rate (nozzle tangential velocity) are used as default settings. However, the extrusion dynamics exhibit nonlinear behavior due to thermal, rheological, and fluid dynamic effects, posing challenges in real-time estimation and modeling of the extrusion rate. Real time sensing of the flow rate is difficult due to the geometry of the nozzle and small observable window, limiting the application of feedback control to the extrusion process.

The extrusion system in filament-based 3D printers starts with a filament shaped feedstock, commonly 1.75 mm in diameter. The nozzle outlet diameter, commonly 0.4 mm, is smaller than the filament. The extruder layout is shown in Figure 1. Due to the difference in the diameters, viscous back pressure is generated as the filament is forced through the nozzle outlet. This induced pressure causes the yet un-

melted filament inside the extruder to buckle and deform. Therefore, as the extruder is driven from rest, a measurable lag or delay is observed until the desired flow rate is achieved. Similarly, as the extruder is driven from steady state operation to rest, there exists a lag until no flow is observed at the orifice exit. Moreover, the length of the delay is not constant, as it fluctuates depending on the back pressure in the extruder. The variable lag may also be affected by temperature fluctuations as heat flows from the heat-block thermal reservoir to melt the polymer feedstock [7]. The impact of under-extrusion and over-extrusion from the lags can be seen in the small gaps at the start of the extrusion line, and as “blobs” at the termination point of the extrusion line in Figure 2.

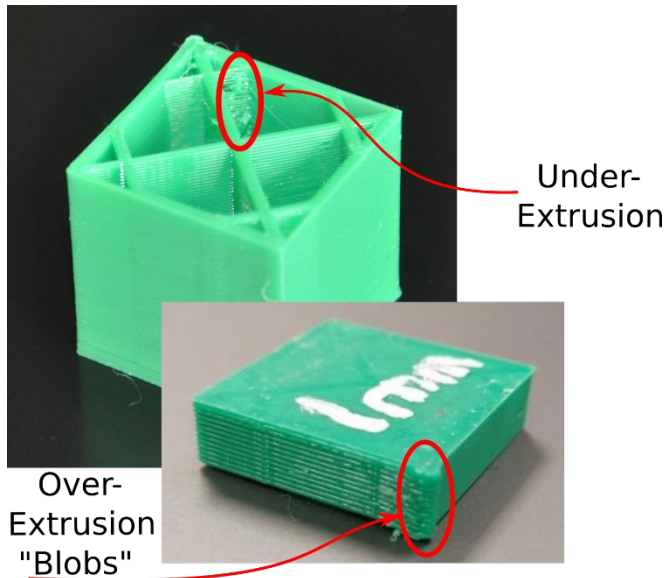


Figure 2. Under-extrusion and over-extrusion defects from poor extrusion control, the cube is of a 20 mm³ size. The poor extrusion control is visible on the transitions from the 0.4 mm bead width on the outer perimeters to the 1.0 mm inner infill.

Prior extrusion control studies focused on applying linear control to linearized extrusion system models. Tronvoll et al. introduced a lead compensator type feedforward control approach that is commonly called “linear advance” in this application. The system model used in [8] is a linear first-order model. The system pole and zero are found experimentally by printing successive lines within a range of input velocities. Similarly, [9] identified a linear model and implemented a lead-lag compensator to provide better reference tracking at acceleration or deceleration conditions, such as in cornering moves, for big area additive manufacturing (BAAM). Both works limit their scope to linear models and controllers. Piny Wu et al. proposed and demonstrated a controller that uses print speed variation (motion control) to achieve better reference tracking on step changes of extrusion reference velocity through feedforward control [6]. Additionally, the researchers implemented a nonlinear system model and a learning controller, which achieved improved performance over a linear controller. The need for accurate modeling and control of extrusion is further motivated by [10], in which continuously varying bead width is employed to reduce voids due to limitations of conventional toolpath slicing algorithms. The successful implementation of the continuously varied extrusion or CONVEX is heavily dependent on comprehensive modeling of the extrusion dynamics to achieve desired bead width at specified positions along the bead [10].

The models used in extrusion control fall into two categories, linear first-order models, and nonlinear mappings of a pole (or its corresponding time constant) to input signal- measured output extrusion speed. Therefore, there exists a need for a comprehensive model that predicts the extruder time constant using prior data of the commanded and associated output extrusion speeds, temperature, X-axis and filament displacement, and extrusion force. In this paper, we present a framework for automated data collection as well as preliminary data that can be used to empirically identify models of FFF extrusion systems.

Methods

Belt 3D Printer:

Belt 3D printers provide the capability of continuous operation and automated part ejection, allowing for automated and successive experiment runs. The components of the system are 1) a belt 3D printer (iFactory One Pro, iFactory3D, Germany), 2) a structured light 3D surface scanner (Gocator 3506A, LMI Technologies, Canada), 3) a document camera stand (Kaiser 5507, Germany). A picture of the experimental system is shown in Figure 3.

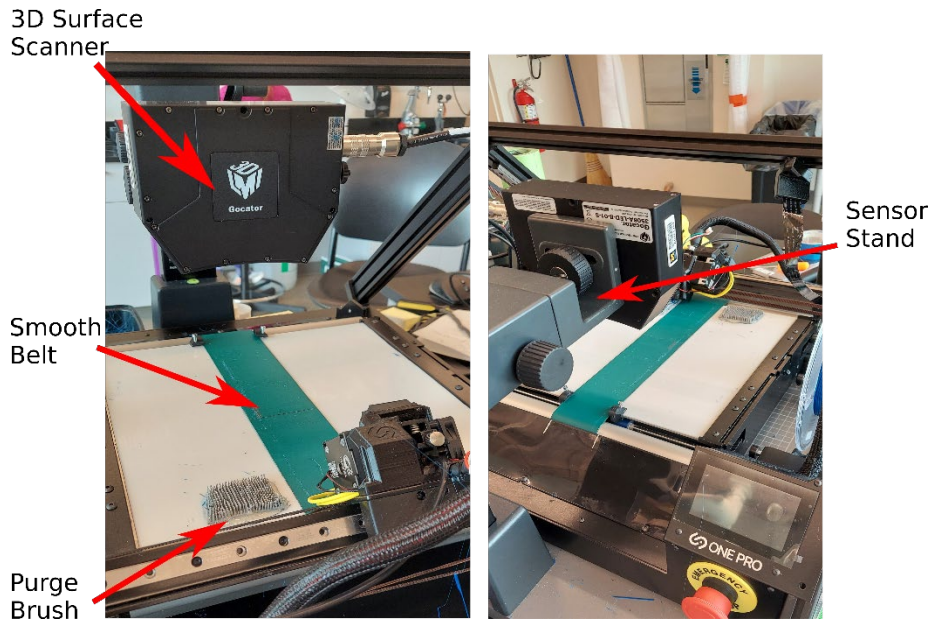


Figure 3. Overview of the experimental automated data collection system

The belt 3D printer was modified for continuous print-scan operation. The original manufacturer supplied belt had a rough surface texture that produced a large number of occlusions in the resulting 3D surface scan. The implemented solution was a custom belt with a smooth top surface. To ensure that any stray pieces of polymer do not get incorporated into the printed pattern, silicone brush pads were installed on each side of the extruder. The nozzle is purged and then brushed against the brushes prior to the printing of each pattern.

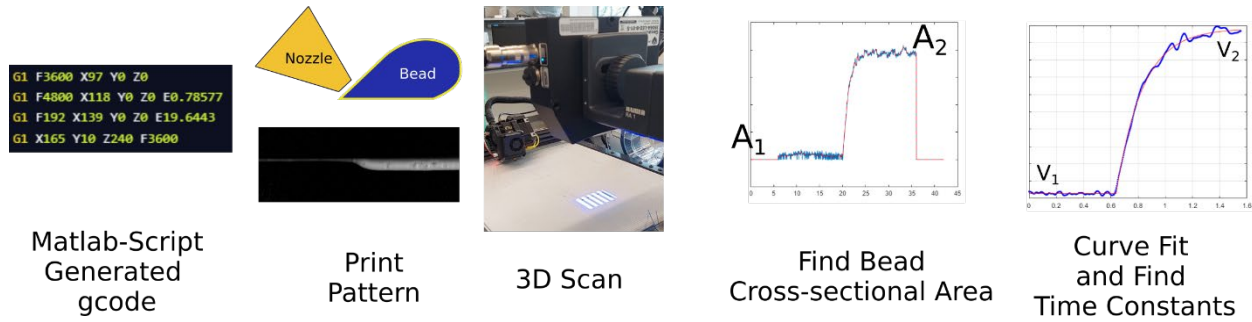


Figure 4. Sequence of experiment steps.

The overall process for identifying the time constants of the system can be summarized in the following steps (Figure 4).

- 1) Generation of the printing instructions in gcode format
- 2) Printing of the gcode file using polylactic acid (PLA) polymer at a temperature of 220 °C
- 3) Scanning of the printed pattern using a structured light 3D scanner.
- 4) Calculation of the bead cross sectional area.
- 5) Curve fitting to the bead cross section area signal and collecting the time constant terms.

The scans that are obtained from the 3D scanner contain a slight curvature that is present in the belt of the 3D printer, in addition to scan occlusions. Therefore, prior to the calculation of the bead cross sectional area, multiple preprocessing steps are required. The first preprocessing step includes filling of occlusions in the 3D scan, the algorithm takes in the average of the values of the 8 pixels that surround the missing pixel and then fills the missing pixel with the average value. Once the scan is filled, the twist in the scan is removed by fitting a first order polynomial surface to fit the twist in the scan and then subtracting the fitted surface from the original scan. The bead area is calculated by taking a row of pixels that cross the bead, and numerically calculating the area underneath, to find the bead cross section area at that slice. The bead cross sectional area is calculated for all the slices of the bead along its length, to obtain the bead area vs. length signal. Following a conversion of the signal from the spatial to the temporal domain, the rise and fall region of the bead area signal are used to fit an exponential rise or fall curve using the following equation:

$$v_{extruder}(t) = a(1 - e^{\frac{t_0-t}{\tau}}) + c \quad (1)$$

Where τ is the value of the fitted time constant in units of seconds. The terms a , t_0 , and c are fitting parameters relating to the value of the exponential function post rise, the initial time of the rise, and the initial value of the signal, respectively. $v_{extruder}(t)$ is the extrusion velocity as a function of time. The entire process is summarized in Figure 5.

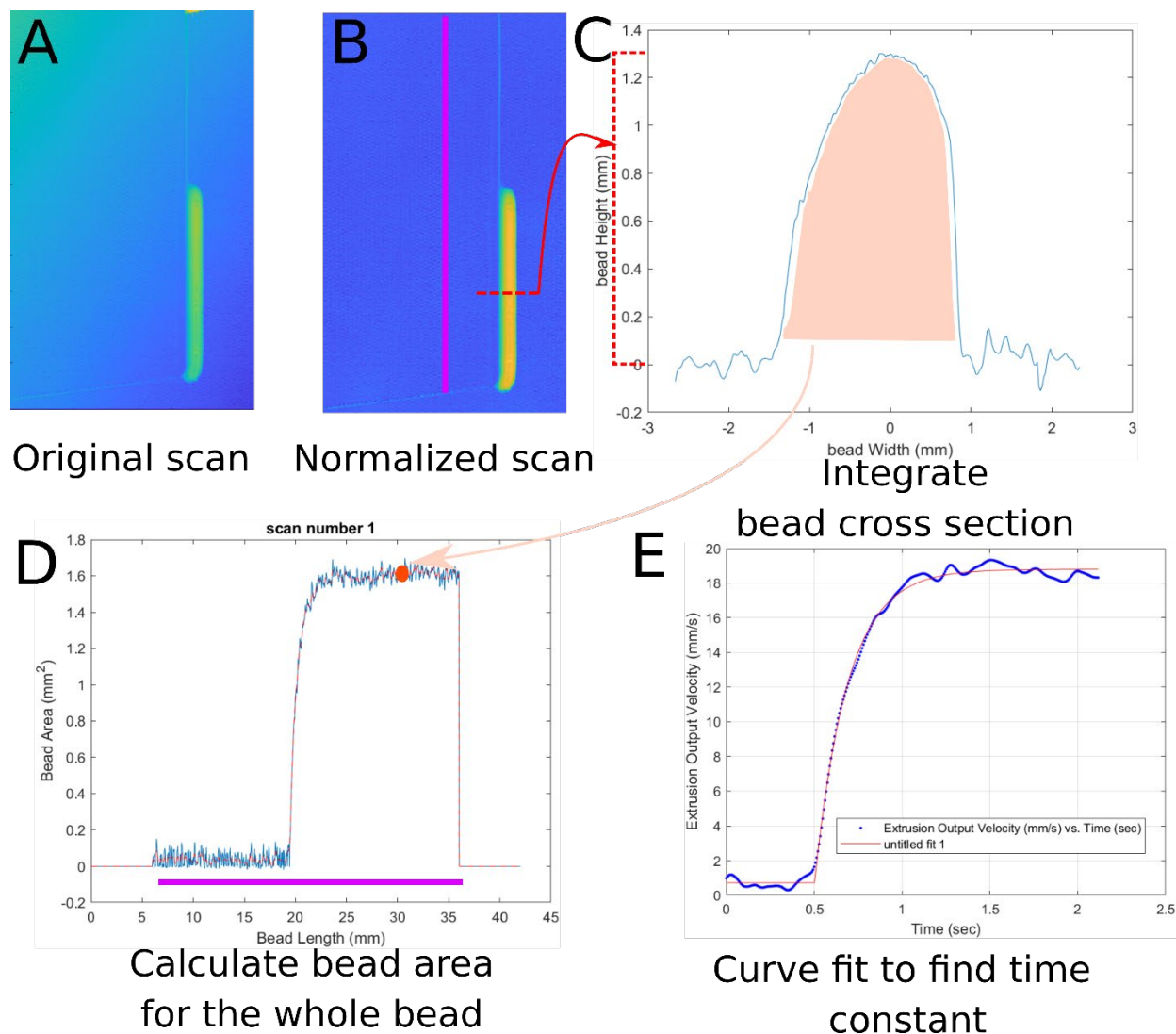


Figure 5. Processing steps of the 3D scans of the printed beads. **(A)** shows the original scan with a warped plane, where the high points are in the upper left corner and the low points are in the lower right corner. **(B)** shows the normalized scan, where the warp in the scan is removed. **(C)** Shows a cross section slice of the bead, the slice is taken from the bead in Panel **B**. The cross-sectional area of the bead (shown in light orange) is numerically integrated. **(D)** shows the bead cross sectional area signal along the length of the bead, as represented by the fuchsia line that is shared with panel **B**. The orange dot represents the bead area that was calculated in panel **C**. **(E)** Shows the exponential fit in red to the extrusion velocity signal in blue.

The test pattern is a single extrusion line, where the extrusion velocity or the X-Axis velocity is varied in a step input signal form. The test pattern is shown in Figure 6.

The extruder inlet velocity can be related to the resulting bead geometry using the conservation of volume principles given by

$$Q_{in} = Q_{out} \quad (2)$$

where Q_{in} is the input flow rate and Q_{out} is the output flow rate. Both flow rates can be represented as,

$$Q_{in} = v_{xy}A_{Bead} \quad (3)$$

$$Q_{out} = v_{extruder}A_{filament} \quad (4)$$

where v_{xy} is the velocity of the 3D printer gantry, $v_{extruder}$ is the extruder velocity or the speed of the filament, and A_{bead} is the bead cross sectional area.

The output velocity of the extruder can be related to the bead cross sectional area using,

$$v_{extruder}A_{filament} = v_{xy}A_{bead} \quad (5)$$

Thus, the area of the resulting extruder velocity from the scanned bead area can be found from,

$$v_{extruder} = \frac{v_{xy}A_{bead}}{A_{filament}} \quad (6)$$

The dynamic system model [6] of the extrusion process can be modeled as a linear first order differential equation, like that of a charging capacitor, with time constant τ as:

$$\dot{v}_{extrusion} + \frac{1}{\tau}v_{extrusion} = \frac{1}{\tau}v_{input} \quad (7)$$

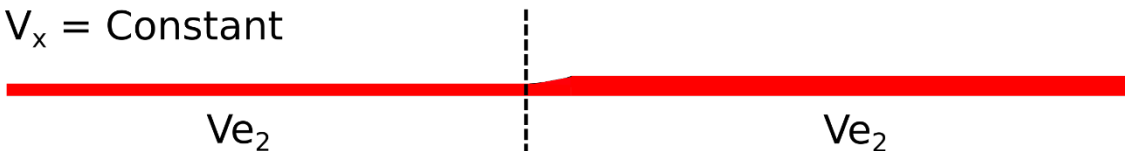
Where v_{input} is the gcode commanded extrusion velocity. The physical system has nonlinearities that cause deviations in τ from (7) due to such factors as temperature of the molten polymer in the nozzle, temperature-dependent viscosity of the molten polymer, shear-rate dependent viscosity of the molten polymer, and time variation in the volume of molten polymer inside the nozzle.

Bead
Cross-section



A: Fixed X-Axis velocity

$V_x = \text{Constant}$



B: Fixed extrusion velocity

$V_e = \text{Constant}$

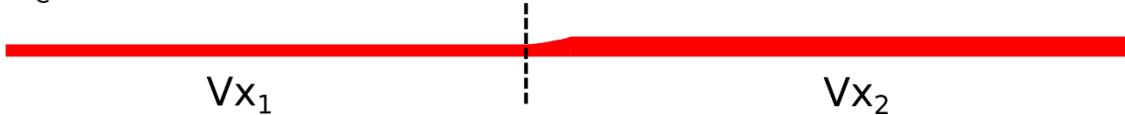


Figure 6. Diagram of experiment test conditions. Condition A holds the X-Axis constant while the extrusion velocity is varied between two values. Condition B holds the extrusion velocity constant while changing the X-Axis velocity to achieve a change in the bead cross section area.

The bead cross sectional area change can be obtained in three ways: 1) by holding the X-Axis velocity constant while increasing the extrusion velocity in a step input format, 2) by holding the extrusion velocity constant while varying the X-Axis velocity, or 3) by a combination of both conditions. In this work, we study fixed X-Axis velocity condition as well as the fixed extrusion velocity condition as shown in Table 1 and Figure 6.

Cartesian 3D printer:

To investigate the transferability of the time constant identification method and resulting data trends to the more common nozzle orientation of 90 degrees, a second printer was tested with a less expensive 2D document scanner to measure bead width. An Original Prusa i3 MK3s+ 3D Printer (Prusa Research, Czech Republic), modified with a V6 Revo extruder and nozzle system (E3D Online, United Kingdom) was used to print patterns with fixed X-Axis velocity condition. The printed lines are scanned using a high-resolution Epson Perfection V600 Photo scanner at a resolution of 2400 dots per inch. The gcode file used for printing was generated using Prusa Slicer version 2.6.0 with the “Arachne” perimeter generator. The “Arachne” perimeter generator allows for continuous variation of the bead width within a single bead. The increase in the bead width is achieved by increasing the flow rate of the filament while holding the X-Axis velocity constant (condition A of Figure 6). The added hardware required to use this identification method is only a high-resolution document scanner which retails for under \$400, whereas the 3D scanner used with the belt printer is more than an order of magnitude more expensive.

The beads were printed using a 0.6 mm outlet brass nozzle with a print speed of 20 mm/s and a layer height (bead height) of 0.2 mm. This speed and bead height are default values for this material and the slow speed is used primarily in first layers to provide good adhesion to the print bed. The commanded bead width variations were from a baseline width of 0.65 mm to bead widths up to 1.20 mm in 0.05 mm increments and from a baseline width of 0.70 mm to bead widths up to 1.05 mm in 0.05 mm increments. The printed bead reaches a steady state over 200 mm of travel before each step in bead width.

The experiment steps are summarized in Figure 7. The build plate used was a standard Prusa smooth poly(ether imide) (PEI) coated spring steel sheet, which has a green tint. The filament used was silver-colored poly(lactic acid) (PLA) (TECBEARS, China). The scan processing steps are background removal by first adjusting the green-magenta tint to full magenta. The color image is then converted to grayscale and then to black-and-white using Otsu’s thresholding method for binarization in MATLAB image processing toolbox. Registration of the image location for the transition in bead width is achieved using two printed centerline beads for this purpose, with automated determination of the midpoints of the centerline beads. The bead width data is captured by cropping to each bead, performing image binarization using Otsu’s method, excluding small regions (noise, perhaps due to polymer stringing), and then counting the pixels in each row of the image. The data transition between bead widths is pre-processed before fitting an exponential decay curve. The pre-processing flips the data if necessary to turn an exponential rise into an exponential decay for automated fitting of time constant. The pre-processing sets the transition time to 0 seconds and then the average bead width of the scan data from 0.3 seconds to 0.8 seconds to zero by uniform subtraction in the data. The curve fit uses the first 0.3 seconds of the data (blue points in Figure 7) for fitting an equation of the form $y = a * \exp(b * x)$, where x is time in

seconds and y is the difference in bead width from the average bead width at $0.3 s < x < 0.8 s$, with data flipped for steps up in bead width. Bead widths are transformed into bead areas using a pill shape model in which a bead is composed of a rectangle with semicircles at its left and right sides, giving $A = (w - h) * h + \pi h^2 / 4$ for bead area A , width w , and height h .

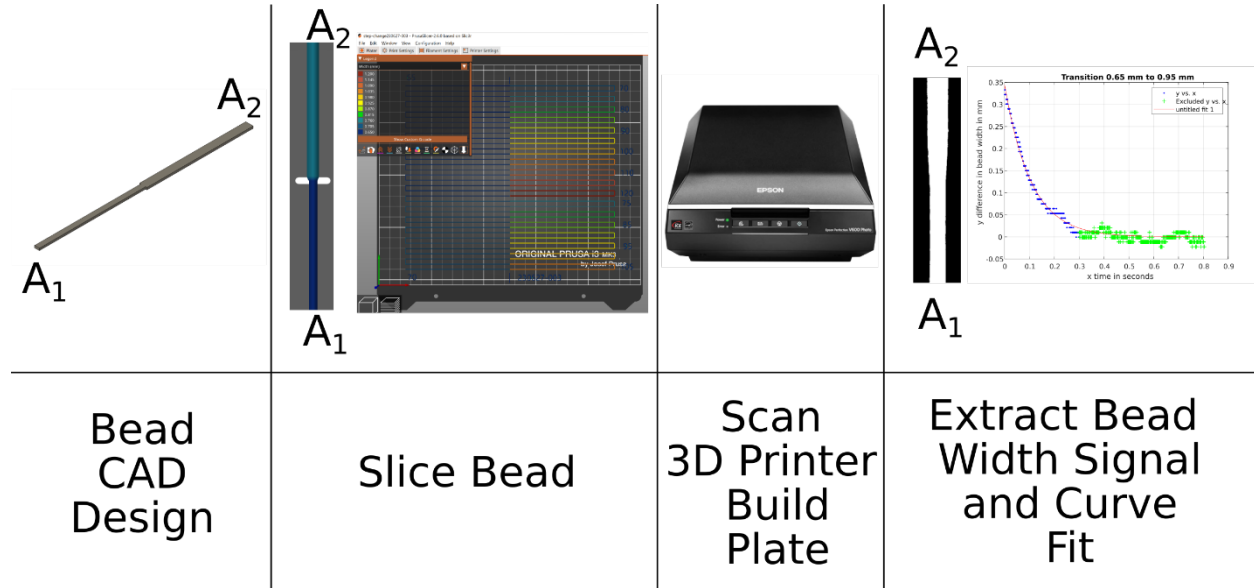


Figure 7. Experiment process steps using Prusa 3D printer and a document scanner.

Results and Discussion

Belt 3D printer:

For each test condition, the experimental conditions of step-up and step-down in bead area for the pair (A_1, A_2) is repeated 6 times. All data are provided in Table 1 and summary plots in Figures 8 and 9 are presented with median and median absolute deviation instead of mean and standard deviation. This presentation is used because some of the automated curve fits of the rise and fall signals obtained from the surface scans gave poor fits that are affected by noise in the bead width signal prior to or after the transient. Noise could be due to stringing, lighting, surface texture, or image processing. These outliers have little effect on median and median absolute deviation. Note that the median absolute deviation is smaller than the standard deviation in a Gaussian distribution, for which one standard deviation is about 1.5 median absolute deviation.

For the fixed X-Axis velocity condition, the time constant exhibits a decrease in magnitude as the jump in bead area magnitude is larger. The opposite trend can be observed for the fixed E-Speed step-up/step-down condition, where the time constant increases as the jump in the speed magnitude is larger. The step-down conditions follow similar trends to the step-up conditions; however, they do not share similar time constant values.

Table 1. Experiment test conditions with corresponding time constant results.

Condition	X-Axis Speed ($V_{Ei} - V_{Ef}$) (mm/s)		E-Axis Speed ($V_{Xi} - V_{Xf}$) (mm/s)		Bead Area ($A_i - A_f$) (mm ²)		Median Time Constant (sec)	MADs
Fixed X-Axis speed (Step up bead area condition)	60	60	2.25	9.73	0.09	0.39	0.2298	0.0380
			2.25	21.20	0.09	0.85	0.1908	0.0193
			2.25	36.67	0.09	1.47	0.1781	0.0107
			2.25	56.13	0.09	2.25	0.1693	0.0137
			9.73	21.20	0.39	0.85	0.1775	0.0234
			9.73	36.67	0.39	1.47	0.1729	0.0100
			9.73	56.13	0.39	2.25	0.1566	0.0056
			21.20	36.67	0.85	1.47	0.1428	0.0090
			21.20	56.13	0.85	2.25	0.1468	0.0102
			36.67	56.13	1.47	2.25	0.1838	0.0227
Fixed X-Axis speed (Step down bead area condition)	60	60	9.73	2.25	0.39	0.09	0.1071	0.0174
			21.20	2.25	0.85	0.09	0.1285	0.0059
			21.20	9.73	0.85	0.39	0.1309	0.0180
			36.67	2.25	1.47	0.09	0.1027	0.0070
			36.67	9.73	1.47	0.39	0.1191	0.0094
			36.67	21.20	1.47	0.85	0.1377	0.0050
			56.13	2.25	2.25	0.09	0.0842	0.0035
			56.13	9.73	2.25	0.39	0.0972	0.0017
			56.13	21.20	2.25	0.85	0.1079	0.0095
			56.13	36.67	2.25	1.47	0.2852	0.0743
Fixed E-Axis speed (Step up bead area condition)	3.67	2.40	2.245	2.245	0.09	0.39	0.1216	0.0160
	6.35	2.40			0.09	0.85	0.1225	0.0126
	6.35	3.67			0.09	1.47	0.1461	0.0068
	13.85	2.40			0.09	2.25	0.1868	0.0042
	13.85	3.67			0.39	0.85	0.1455	0.0173
	13.85	6.35			0.39	1.47	0.1889	0.0037
	60	2.40			0.39	2.25	0.2405	0.0032
	60	3.67			0.85	1.47	0.2701	0.0369
	60	6.36			0.85	2.25	0.2687	0.0185

	60	13.85		1.47	2.25	0.3150	0.0129	
Fixed E-Axis speed (Step down bead area condition)	2.40	3.67	2.245	2.245	0.39	0.09	0.0668	0.0269
	2.40	6.35			0.85	0.09	0.0787	0.0140
	2.40	13.85			0.85	0.39	0.1416	0.0128
	2.40	60			1.47	0.09	0.0994	0.0064
	3.67	6.35			1.47	0.39	0.1523	0.0166
	3.67	13.85			1.47	0.85	0.1960	0.0329
	3.67	60			2.25	0.09	0.1213	0.0049
	6.35	13.85			2.25	0.39	0.1708	0.0088
	6.35	60			2.25	0.85	0.2344	0.0110
	13.85	60			2.25	1.47	0.2533	0.0503

The time constant data in Table 1 is plotted for the fixed extrusion velocity and fixed X-Axis velocity conditions in Figure 7 and Figure 8, respectively.

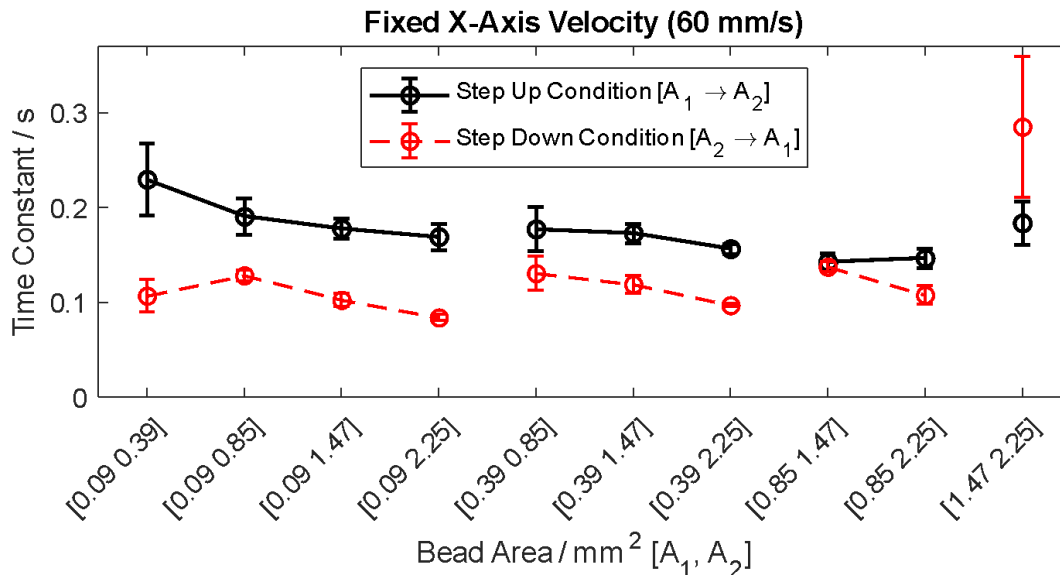


Figure 8. Time constant values for step down and step up in bead area with fixed X-Axis velocity experiment condition.

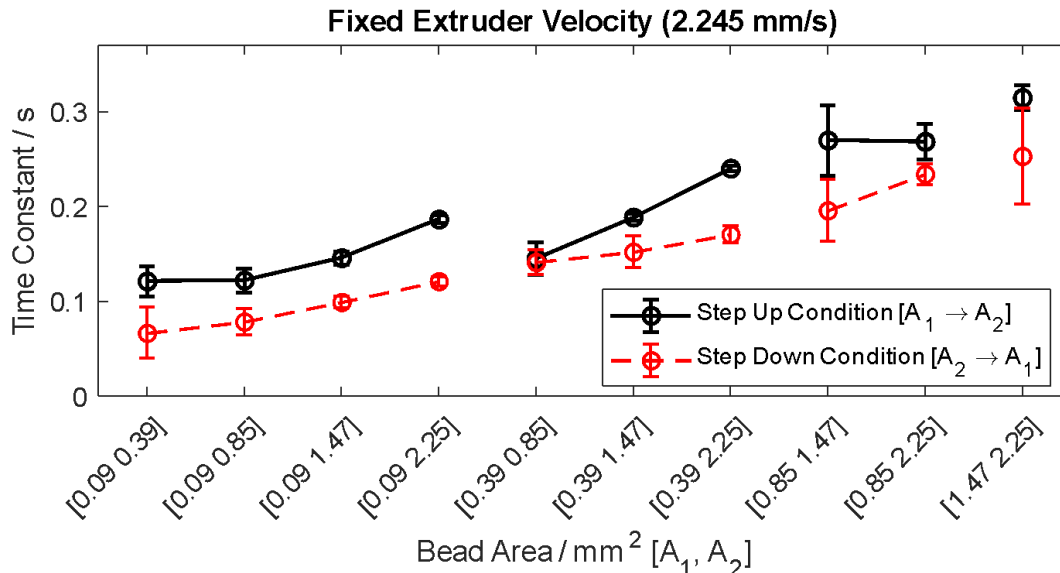


Figure 9. Time constant values for step down and step up in bead area with fixed extrusion velocity experiment condition.

Cartesian 3D Printer:

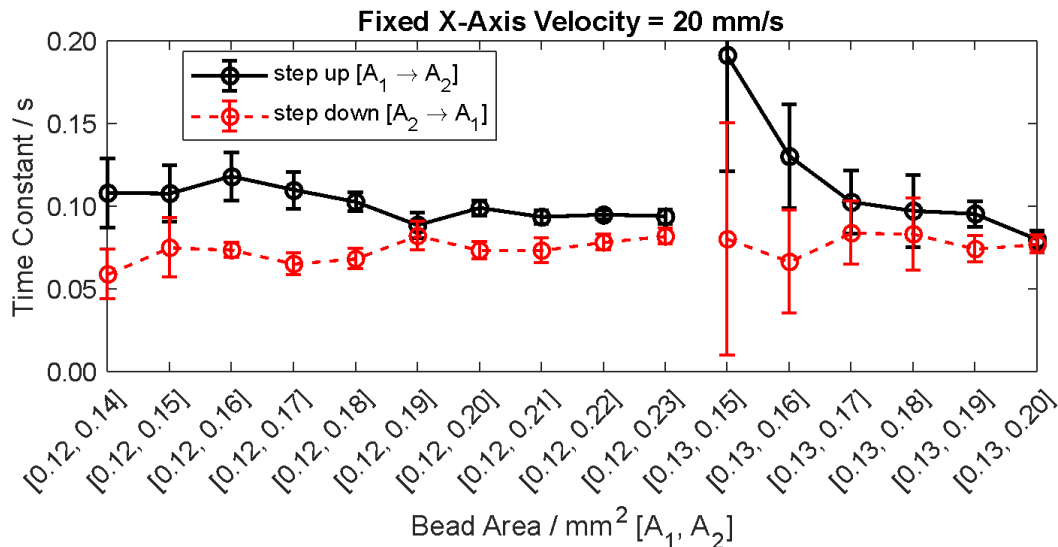


Figure 10. Time constant values for step down and step up in bead area with fixed X-Axis velocity using the cartesian 3D printer.

A summary plot for the Cartesian printer is provided in Figure 10. Small steps in bead width (0.05 mm or 0.10 mm) were difficult to resolve in this procedure and are excluded from summary analysis. Note that the pixel resolution of the scan with scan resolution 2400 dots per inch is 0.016 mm per pixel, so a 0.100 mm bead width step is discretized into 6 pixels of bead width change.

The measured time constant for a rise (step up) in bead width has a negative correlation with step height (or with end bead width) for steps to 0.85 mm and above from a starting bead width of 0.65 mm. The measured time constant for a fall (step down) in bead width may have a slight positive correlation with step size (or with start bead width), although the uncertainty in the measurements indicates a need for a

more precise measurement. Notice also that the measured time constant for a fall (A_2 to A_1) was usually less than the measured time constant for the corresponding rise (A_1 to A_2), moreover, it was observed that the measured time constants typically have lower stochasticity for larger steps in bead width. There may be a point at high enough steps that the step-up and step-down time constants become equal or even cross over.

Conclusion

This work is aimed at building a framework for large data collection of the extrusion system parameters for use in data driven modeling of the extrusion behavior and spreading of polymer melts in FFF. This paper presents the first step in this direction, as well as some preliminary data that supports the nonlinearity behavior claims of the extrusion process. The time constants extracted from the fixed X-Axis velocity experiments show an overall reduction in time constant magnitude as the steps in extrusion velocity are higher. This trend is shared across both 3D printing setups. The fixed extrusion velocity experiments, however, show the opposite trend, where the time constant increases in magnitude as the steps in velocity are higher. Another shared observation between both 3D printing setups is the difference in the value of time constant between the step-up and step-down condition, while sharing a similar overall trend. The results of these preliminary experiments show the shortcoming of using one value of time constant as a model parameter for the whole print in combination with a linear controller, as the time constant changes wildly for different regions of the print. These experiments also show the need for comprehensive system identification experiments to build a comprehensive model of the extrusion system, which will allow for better controllability of the extrusion system and produce fewer printing errors.

References

- [1] “ISO/ASTM 52900:2021(en), Additive manufacturing — General principles — Fundamentals and vocabulary.” <https://www.iso.org/obp/ui/#iso:std:iso-astm:52900:ed-2:v1:en> (accessed May 15, 2023).
- [2] F. Rengier *et al.*, “3D printing based on imaging data: Review of medical applications,” *Int J Comput Assist Radiol Surg*, vol. 5, no. 4, pp. 335–341, May 2010, doi: 10.1007/S11548-010-0476-X/METRICS.
- [3] B. J. Tuazon, N. A. V. Custodio, R. B. Basuel, L. A. D. Reyes, and J. R. C. Dizon, “3D Printing Technology and Materials for Automotive Application: A Mini-Review,” *Key Eng Mater*, vol. 913, pp. 3–16, 2022, doi: 10.4028/P-26O076.
- [4] A. Bellini, S. Güçeri, and M. Bertoldi, “Liquefier Dynamics in Fused Deposition,” *J Manuf Sci Eng*, vol. 126, no. 2, pp. 237–246, May 2004, doi: 10.1115/1.1688377.
- [5] I. J. Solomon, P. Sevel, and J. Gunasekaran, “A review on the various processing parameters in FDM,” *Mater Today Proc*, vol. 37, no. Part 2, pp. 509–514, Jan. 2021, doi: 10.1016/J.MATPR.2020.05.484.
- [6] P. Wu, K. S. Ramani, and C. E. Okwudire, “Accurate linear and nonlinear model-based feedforward deposition control for material extrusion additive manufacturing,” *Additive Manufacturing 2021, Vol. 48, Page 102389*, vol. 48, p. 102389, Oct. 2021, doi: 10.1016/J.ADDMA.2021.102389.
- [7] A. Bellini, S. Güçeri and M. Bertoldi, "Liquefier Dynamics in Fused Deposition", *Journal of Manufacturing Science and Engineering*, vol. 126, no. 2, pp. 237-246, 2004. doi: 10.1115/1.1688377.
- [8] S. Tronvoll, S. Popp, C. Elverum and T. Welø, "Investigating pressure advance algorithms for filament-based melt extrusion additive manufacturing: theory, practice and simulations", *Rapid Prototyping Journal*, vol. 25, no. 5, pp. 830-839, 2019. doi: 10.1108/rpj-10-2018-0275.
- [9] P. Chesser *et al.*, "Extrusion control for high quality printing on Big Area Additive Manufacturing (BAAM) systems", *Additive Manufacturing*, vol. 28, pp. 445-455, 2019. doi: 10.1016/j.addma.2019.05.020.
- [10] A. Moetazedian, A. Budisuharto, V. V. Silberschmidt, and A. Gleadall, “CONVEX (CONtinuously Varied EXtrusion): A new scale of design for additive manufacturing”, *Additive Manufacturing*, vol. 37, 2021. doi: 10.1016/j.addma.2020.101576

Data Availability Statement

The print planning (3MF) files used for slicing gcode in the Cartesian 3D printing experiments are available here: <https://www.printables.com/model/516417-calibration-prints-for-determining-time-constant-o>